Accurate Ratio Computation using Abstract Chemical Reaction Networks

Iuliia Zarubiieva, Joyun Tseng, and Vishwesh Kulkarni

***Abstract*—We present new results on how abstract chemical reactions, viz., catalysis, annihilation and degradation, can be used to implement circuits that accurately compute ratio of two input signals. The input signals can be either constant-valued scalars or time-varying scalars or polynomials. We also characterise the robustness of our circuits to parameter variations, as would be encountered in wet-lab implementations.**

***Index Terms*—abstract chemical reaction network, DNA strand displacement, stability, robustness, Circle criterion**

I. Introduction

An objective of synthetic biology is to design biomolecular circuits for *in situ* monitoring and control. Recently, nucleic acid reactions have been proposed as a potential solution for these purposes [1], [2], [3], [4]. A key advantage of nucleic acid reactions consists in the ease and precision with which these can be implemented, as their design relies essentially on the well-known Watson-Crick base-pairing mechanism (i.e. adenine-thymine and guanine-cytosine pairing), which enables precise programming and timing of molecular interactions simply by the choice of relevant sequences. This approach has allowed the implementation of a number of complex circuits based on DNA strand displacement [5], DNA enzyme [6] and RNA enzyme [7] reactions, and has been used for the modelling and implementation of various nucleic-acids-based circuits such as feedback controllers [8] and predator-prey systems [9]. Recently, it has been shown that any *chemical reaction network* can be closely approximated by a set of suitably designed DNA strand displacement reactions [10]. This logic can be extended to approximate a set of linear ordinary differential equations (ODEs) by a set of idealised *abstract chemical reaction networks* (ACRNs) which can then be approximated by a set of suitably designed DNA strand displacement reactions [4]. In [11], it was shown that ACRNs for catalysis using two reactants can be used to realise a set of nonlinear operators and, in particular, was used to implement a system $\mathscr{S}_D$ that computes the ratio of two entities - these entities can be two constant-valued scalars or two time-varying signals or two constant-valued polynomials or two time-varying polynomials. However, $\mathscr{S}_D$ suffers from steady-state errors. In this paper, we present two circuits, viz., $\mathscr{S}_{C1}$ (see Fig. 1) and $\mathscr{S}_{C2}$ (see Fig. 2) to overcome this limitation. We also characterise the input-output stability of $\mathscr{S}_{C1}$. Our circuits can be implemented in the wet-lab using DNA strand displacement on the lines described in [4]. In practice, DNA/RNA deactivate rapidly with time, typically with a half-life of 15 minutes, leading to appreciable time delays in the feedback loop which render the feedback system unstable. Hence, we also characterise the tolerance of $\mathscr{S}_{C1}$ to the time-delays.

Manuscript received April 08, 2018. This work was supported in part by the EPSRC INDUSTRIAL CASE AWARD 16000070, Microsoft Research, and the EPSRC-BBSRC grant to the Warwick Integrative Biology Centre.

Iuliia Zarubiieva, Joyun Tseng, and Vishwesh Kulkarni are with the School of Engineering, University of Warwick, Coventry, CV4 7AL, UK. E-mail: I.Zarubiieva@warwick.ac.uk, J.Tseng.1@warwick.ac.uk, V.Kulkarni@warwick.ac.uk .

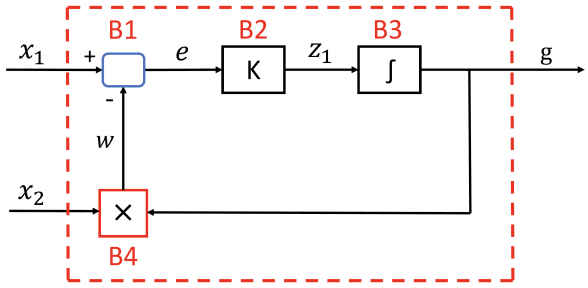

Fig. 1: $\mathscr{S}_{C1}$**:** *Block diagram for our first circuit for accurately computing the ratio $g = x_1/x_2$. This system takes 2 inputs, viz., x_1 and x_2, and produces the output g. The inputs need not be constant and are allowed to be time-varying. We refer to the blocks B1 and B2 taken together as B1+B2.*

II. Notation and Background Results

To ensure consistency, the notation used in [12] and [4] is used throughout in this paper. For example, a bidirectional (i.e., a reversible bimolecular chemical reaction) is represented as

$$X_1 + X_2 \underset{\delta_2}{\overset{\delta_1}{\rightleftharpoons}} X_3 + X_4 \tag{1}$$

where X_i are chemical species with X_1 and X_2 being the reactants and X_3 and X_4 being the products. Here, δ_1 and δ_2 denote the forward and backward reaction rates, respectively. A unimolecular reaction features only one reactant whereas a multimolecular reaction features two or more reactants. Degradation of a chemical species X at rate K (or conversion of X into an inert form at a rate K) is denoted by $X \xrightarrow{K} \emptyset$.

A. Representing signals using differences of concentrations

Whereas signals in systems theory can take both positive and negative values, biomolecular concentrations (with Molar (M) as unit) can only take non-negative values. Thus, following the same approach suggested in [12] and [4], we represent a signal, x as the difference in concentration of two chemical species, x^+ and x^-. Here, x^+ and x^- are respectively the positive and negative components of x such that $x = x^+ - x^-$. The consequence of adopting this scheme is that there is no unique representation for a particular signal. As an example, $x = 20$ M can be represented by both $x^+ = 50$ M and $x^- = 30$ M or equivalently, $x^+ = 20$ M and $x^- = 0$ M. In practice,

ISBN: 978-988-14047-9-4
ISSN: 2078-0958 (Print); ISSN: 2078-0966 (Online)

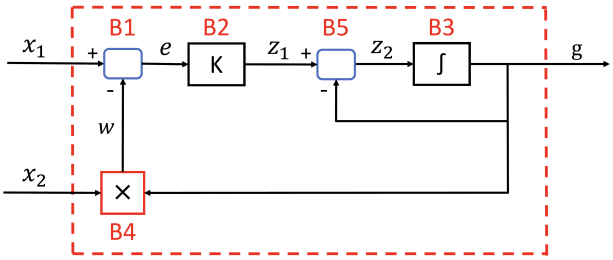

Fig. 2: $\mathscr{S}_{C2}$**:** *Block diagram for our second circuit for accurately computing the ratio $g = x_1/x_2$. Here, the integrator of $\mathscr{S}_{C1}$ is replaced by a low-pass filter. This system takes 2 inputs, viz., x_1 and x_2, and produces the output g. The inputs need not be constant and are allowed to be time-varying.*

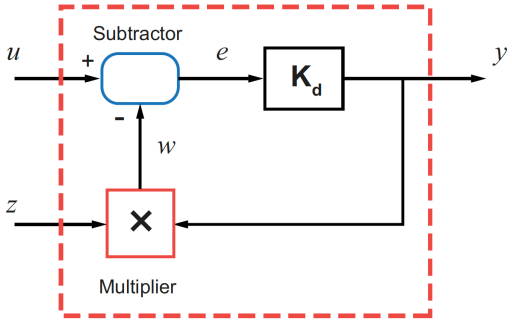

Fig. 3: A block diagram representation of the feedback system $\mathscr{S}_D$ of [11] that computes the ratio $y = u/z$ where u and z are biomolecular signals.

x^+ and x^- can be realised as single strand DNA molecules, as illustrated in [4] where these complementary positive and negative components would annihilate each other at reaction rate η (i.e. $x^+ + x^- \xrightarrow{\eta} \emptyset$). A key advantage of using this scheme is that it allows the realisation of the 'subtraction' operation, as discussed further below.

B. Realising elementary linear system theoretic operators

In [12], results on how to represent linear system theoretic operations such as gain, summation and integration using idealised abstract chemical reactions are presented and it is shown that only three types of elementary chemical reactions, namely, catalysis, annihilation and degradation are needed for such representations. In [4], this set of elementary chemical reactions is further reduced to only two. We here summarise their main results and refer the interested reader to [12] and [4] for details.

Throughout the rest of the paper, equations with superscript $\pm$ and $\mp$ are used as shorthand notations that represent the '+' and '−' individual reactions — for example, $x_i^\pm \xrightarrow{K} x_i^\pm + x_o^\pm$ should be understood as the the set of two reactions: $x_i^+ \xrightarrow{K} x_i^+ + x_o^+$ and $x_i^- \xrightarrow{K} x_i^- + x_o^-$. Likewise, the notation $x_i^\pm \xrightarrow{K} x_i^\pm + x_o^\mp$ is used to represent the set of two reactions: $x_i^+ \xrightarrow{K} x_i^+ + x_o^-$ and $x_i^- \xrightarrow{K} x_i^- + x_o^+$. For brevity and following [12], we will represent such a set of reactions compactly as $x_i^\pm \xrightarrow{K} x_i^\pm + x_o^\pm$ and $x_i^\pm \xrightarrow{K} x_i^\pm + x_o^\mp$.

As noted in [12], one limitation of representing signals as the difference of concentrations is that the requirement of having the same reaction rate, K, for both positive and negative components may not be easy to implement experimentally. However, as shown in [12], this requirement can be relaxed if the annihilation rate, η in the annihilation reaction, $x_o^+ + x_o^- \xrightarrow{\eta} \emptyset$ is chosen to be sufficiently large. Hence, we assume this condition of $\eta \gg K$ throughout the rest of this paper.

Lemma 1. [Scalar gain K]
Let $x_o = Kx_i$ where x_i is the input, x_o is the output and K is the gain. This operation is implemented using the following set of abstract chemical reactions:

$$x_i^\pm \xrightarrow{\gamma K} x_i^\pm + x_o^\pm, \qquad x_o^\pm \xrightarrow{\gamma} \emptyset, \qquad x_o^+ + x_o^- \xrightarrow{\eta} \emptyset,$$

where γK, γ and η are the kinetic rates associated with catalysis, degradation and annihilation respectively. □

Proof: Using mass-action kinetics, it follows that the gain operator realised in this manner is described using the following ODE,

$$\begin{aligned}
\frac{dx_o^+}{dt} &= \gamma(Kx_i^+ - x_o^+) - \eta x_o^+ x_o^- \\
\frac{dx_o^-}{dt} &= \gamma(Kx_i^- - x_o^-) - \eta x_o^+ x_o^- \\
\frac{dx_o}{dt} &= \frac{dx_o^+}{dt} - \frac{dx_o^-}{dt} = \gamma(Kx_i - x_o)
\end{aligned} \tag{2}$$

Using the final value theorem, the steady state value of x_o for constant input x_i is given by $\lim_{t\to\infty} x_o(t) = Kx_i(t)$. □

Lemma 2. [Summation]
Consider the summation operation $x_o = x_i + x_d$, where x_i and x_d are the inputs and x_o is the output. This operation is implemented using the following set of abstract chemical reactions:

$$x_i^\pm \xrightarrow{\gamma} x_i^\pm + x_o^\pm, \quad x_d^\pm \xrightarrow{\gamma} x_d^\pm + x_o^\pm, \quad x_o^\pm \xrightarrow{\gamma} \emptyset, \quad x_o^+ + x_o^- \xrightarrow{\eta} \emptyset.$$

Using the following set of abstract chemical reactions:

$$x_i^\pm \xrightarrow{\gamma} x_i^\pm + x_o^\pm, \quad x_d^\pm \xrightarrow{\gamma} x_d^\pm + x_o^\mp, \quad x_o^\pm \xrightarrow{\gamma} \emptyset, \quad x_o^+ + x_o^- \xrightarrow{\eta} \emptyset,$$

the subtraction $x_o = x_i - x_d$ is implemented. □

Remark 1. Scaled summation $x_o = K(x_i + x_d)$, and scaled subtraction, can be implemented by choosing the catalysis rates in the construct of Lemma 2 to be $K\gamma$. □

Lemma 3. [Scaled Integration]
Consider the integrator $x_o = K\int x_i\,dt$ where x_i is the input, x_o is the output, and K is the DC gain. Using the following set of abstract chemical reactions:

$$x_i^\pm \xrightarrow{K} x_i^\pm + x_o^\pm, \quad x_o^+ + x_o^- \xrightarrow{\eta} \emptyset,$$

such an integrator is implemented. □

Proof: Using generalised mass-action kinetics the ODEs for the summation and integrator operations are given by $\frac{dx_o}{dt} = \gamma(x_i + x_d - x_o)$ and $\frac{dx_o}{dt} = Kx_i$, respectively. Then, the proof for Lemmas 2 and 3 can be trivially obtained following the same logic as for the proof of Lemma 1. □

In [11], circuit to compute the ratio of any given two numbers was derived. The circuit is shown in Fig. 3 and the result is as follows.

ISBN: 978-988-14047-9-4
ISSN: 2078-0958 (Print); ISSN: 2078-0966 (Online)
(revised on 9 May 2018)

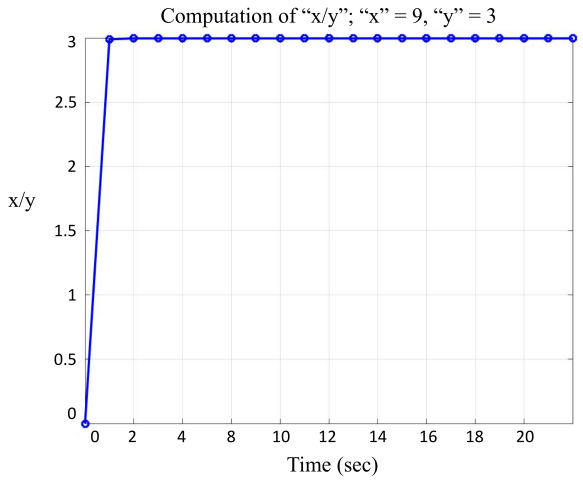

Fig. 4: *Computation of the ratio "9/3" using $\mathscr{S}_{C1}$ for the initial conditions noted down in Fig. 5.*

Lemma 4. [Divider of [11]]
Consider the system $\mathscr{S}_D$ shown in Fig. 3. Let the biomolecular signals u and z be its inputs. Then for sufficiently large values of K_d, its output y approximates the ratio u/z. □

Proof: From Fig. 3, we have $e = u - zy$ and $y = K_d e$. Substituting the former equation into the latter and rearranging the variables, we get $y = K_d(u - yz) = \frac{K_d u}{1+K_d z} = \frac{u}{(1/K_d)+z}$. If K_d is chosen large enough, $y \approx u/z$. □

Remark 2. The Newton-Raphson method can also be used to implement the ratio x/y of two numbers as follows. Define $f(z) = y - 1/z$. Next, starting with an arbitrarily chosen initial condition z_0, compute $1/y$ using the iteration

$$\begin{aligned} z_{n+1} &= z_n - \frac{f(x_n)}{f'(x_n)} \\ &= z_n(2 - y \cdot z_n), \end{aligned}$$

where $f'(\zeta)$ denotes the derivative of $f(\zeta)$ with respect to ζ. Let $\bar{z} = \lim_{n\to\infty} z_n$. Then, the ratio $x/y = x \cdot \bar{z}$. The Newton-Raphson method exhibits a quadratic convergence towards the steady-state value $\bar{z}$. This implementation requires one subtraction operation, one integration operation, and three multiplication operations. In contrast, $\mathscr{S}_D$ requires only one scaled subtractor, one integrator, and one multiplier. □

III. Main Result

In [11], the stability and robustness properties of $\mathscr{S}_D$ were not analysed. Furthermore, the ratio computation using the circuit $\mathscr{S}_D$ incurs a steady state error since it can compute the ratio precisely if and only if K_d is arbitrarily large. In practice, reaction rates are finite and hence a wet-lab implementation of $\mathscr{S}_D$ will always incur a steady-state error. We now present two circuits, viz., $\mathscr{S}_{C1}$ and $\mathscr{S}_{C2}$, that can overcome this limitation: $\mathscr{S}_{C1}$ is shown in Fig. 1 and $\mathscr{S}_{C2}$ is shown in Fig. 2. The ODE representation, the corresponding ACRN representation, and the corresponding DNA implementation for $\mathscr{S}_{C1}$ is given in Table II (see Appendix). As Fig. 4 shows, this circuit computes the ratio precisely and without exhibiting any overshoot if the circuit parameter set is the initially chosen set of parameter values tabulated in Fig. 5. For poorly chosen parameter values, the circuit is unstable and cannot compute the ratio accurately. We now characterize the robustness and stability of $\mathscr{S}_{C1}$.

TABLE I: Notation

Symbol	Meaning
$(\mathbb{R}^+)$ $\mathbb{R}$	Set of all (nonnegative) real numbers.
$x \cdot y$	Product of x and y.
$(\cdot)'$ or $(\cdot)^T$	Transpose of a vector or a matrix $(\cdot)$.
$\langle x, y\rangle$	$= \int_{-\infty}^{\infty} y^T(t)x(t)dt$.
$\|x\|$	$= \sqrt{\langle x, x\rangle}$.
$\mathscr{L}_2$	Space of possibly vector valued signals x. for which $\|x\| < \infty$.
$\mathrm{Re}\,G$ $(\mathrm{Im}\,G)$	Real (imaginary) part of G.
$\dot{x}$	Derivative of x w.r.t. time, i.e., $\frac{dx}{dt}$.
$\measuredangle G$	Angle of a complex number G.

Our notation is summarized in Table I; for the discrete time case, the integration terms are to be appropriately replaced by summation terms, and the discrete time counterpart of $\mathscr{L}_2$ is referred to as ℓ_2. The set of all N-dimensional real-valued vectors is denoted $\mathbb{R}^N$. We refer to an operator by using a capital letter symbol, such as H, whereas a signal is referred to by using a small letter symbol, such as x. Our short-hand notation for $x(t) = 0\ \forall t$ is $x \equiv 0$.

Definition 1. [finite-gain stability] *A system $\mathscr{S}$ mapping $u \in \mathscr{L}_2$ into $y \in \mathscr{L}_2$ is said to be* finite gain stable *if there exists $\gamma \geq 0$ such that $\|y\| \leq \gamma\|u\|$ for all $u \in \mathscr{L}_2$. The smallest value of such a γ is said to be the* gain *of $\mathscr{S}$.* □

Definition 2. [sector] *We say that H is a sector $[k_1, k_2]$ operator if it holds that $\langle Hx - k_1 x, Hx - k_2 x\rangle \leq 0$ for all $x \in \mathscr{L}_2$.* □

Lemma 5 is a straightforward application of the Nyquist stability theorem [13].

Lemma 5. Consider $\mathscr{S}_{C1}$. Let γ_1 be the rate of catalysis and degradation at the scaled summation junction. Let γ_2 be the rate of catalysis at the integrator. Let x_1 be an arbitrary time-varying signal in sector$(0, \alpha)$ and let x_2 be a constant, where $\alpha > 0$. Define

$$G(s) = \frac{K\, x_2\, \gamma_1\, \gamma_2}{s\,(s + \gamma_1)}. \tag{3}$$

Then, $\mathscr{S}_{C1}$ is stable if and only if the Nyquist plot of $G(s)$ does not encircle the point $-1 + j0$ as ω varies from $-\infty$ to ∞. Furthermore, it can tolerate a time-delay of PM/ω_g, where PM denotes the phase margin of $G(s)$ and ω_g denotes the gain cross-over frequency of $G(s)$. Replacing $G(s)$ given by (3) with

$$\widetilde{G}(s) \doteq \frac{K\, x_2\, \gamma_1\, \gamma_2}{(s + \gamma_1)\,(s + \gamma_2)},$$

similar result is obtained for $\mathscr{S}_{C2}$. □

Remark 3. As a result of Lemma 5, the finite gain stability of our ratio computation circuit $\mathscr{S}_{C1}$ is not independent of the denominator x_2 and, in particular, the stability margin decreases with an increase in x_2. □

Remark 4. Lemma 5 illustrates the main challenge posed by ACRN implementations, viz., an increase in the order of the loop transfer function: in the ODE representation of $\mathscr{S}_{C1}$, it

ISBN: 978-988-14047-9-4
ISSN: 2078-0958 (Print); ISSN: 2078-0966 (Online)
(revised on 9 May 2018)

Block	Corresponding catalysis rate	Initially set values	Sets of parameter variations simulated by us: 15 sets in all							
			# 1	# 2	# 3	# 4	# 5	# 6	# 7	# 8
B1	γK1	0.01	**0.1**	**1**	0.01	0.01	0.01	0.01	0.01	0.01
B2	γK2	100	100	100	**1000**	**10000**	**10**	100	100	100
B3	γK3	100	100	100	100	100	100	100	**150**	**500**
B4	γK4	10	10	10	10	10	10	10	10	10
B2	K	250	250	250	250	250	250	**25**	250	250
Settling time, t.u.		1	-	-	1	1	4	8	1	1
Peak overshoot		-	-	-	-	-	-	-	-	-
Computed steady-state value of the ratio "9/3"		2.996005	**unstable**	**unstable**	2.996005	2.996005	2.996005	2.960529	2.996005	2.9960

Block	Corresponding catalysis rate	Initially set values	Sets of parameter variations simulated by us: 15 sets in all						
			#9	# 10	# 11	# 12	# 13	# 14	# 15
B1	γK1	0.01	**0.1**	0.01	**0.1**	**0.1**	**0.001**	0.01	0.01
B2	γK2	100	100	100	100	100	100	100	100
B3	γK3	100	**500**	100	**500**	**500**	100	**10**	100
B4	γK4	10	10	10	**100**	**100**	10	10	**100**
B2	K	250	250	**500**	250	**500**	250	250	250
Settling time, t.u.		1	-	2	1	-	5	6	7
Peak overshoot		-	4.9	-	-	-	-	-	-
Computed steady-state value of the ratio "9/3"		2.996005	3.1510	**2.9980**	2.996005	2.828692	2.995997	2.995991	2.995990

Fig. 5: *Tabulated steady-state response of $\mathscr{S}_{C1}$ for different sets of parameters values; the* time unit *(t.u.) is in seconds. All other factors being equal, an increase in a parameter value should be interpreted as a speed-up of the feedback loop of $\mathscr{S}_{C1}$ and a decrease in the parameter value should be interpreted as a slow-down of the feedback loop of $\mathscr{S}_{C2}$.*

is $G(s) = \frac{K\,x_2}{s}$ but in the ACRN implementation, it is given by $G(s) = \frac{K\,x_2}{s}\left(\frac{\gamma_1\,\gamma_2}{s+\gamma_1}\right)$. Consequently, the ACRN representations have diminished stability and robustness properties compared to their ODE counterparts. □

Remark 5. In principle, $\mathscr{S}_{C1}$ computes the ratio of any two given entities x_1 and x_2 accurately so long as these are either (1) pairs of constant-valued scalars or (2) time-varying scalars or (3) constant-valued polynomials or (4) time-varying polynomials. However, in practice, this can be claimed for only a smaller subset due to the limitations on how fast and how accurately the DNA strand displacement implementation can proceed in the real-world. For example, to compute x_1/x_2 when x_2 is significantly large, γ_1 and γ_2 must be chosen to be proportionately small while ensuring that γ_2 is much larger than γ_1. In practice, since γ_1 and γ_2 are the catalysis rates, these cannot be chosen to be arbitrarily small or large and consequently, $\mathscr{S}_{C1}$ will be unstable if x_2 is chosen to be large enough. Our Lemma 5 establishes how large x_2 can be for which $\mathscr{S}_{C1}$ is finite gain stable. □

Theorem 1. [Stability Analysis of $\mathscr{S}_{C1}$]
Consider $\mathscr{S}_{C1}$. Let γ_1 be the rate of catalysis and degradation at the scaled summation junction. Let γ_2 be the rate of catalysis at the integrator. Let γ_3 be the rate of catalysis and degradation at the multiplication junction. Let x_1 be an arbitrary time-varying signal in sector$(0,\alpha)$ and let x_2 be an arbitrary time-varying signal in sector$(0,\beta)$, where $\alpha > 0$ and $\beta > 0$ are constants. Define

$$G(s) = \frac{K\,\gamma_1\,\gamma_2\,\gamma_3}{s\,(s+\gamma_1)(s+\gamma_3)}. \tag{4}$$

Then, $\mathscr{S}_{C1}$ is stable if and only if

$$\mathrm{Re}\,G(j\omega) > -\frac{1}{\beta} \qquad \forall \omega \in \mathbb{R}. \tag{5}$$

Furthermore, the maximum delay τ^* for which $\mathscr{S}_{C1}$ is stable is given as

$$\tau^* = \frac{\mathrm{PM} - \cos^{-1}(-1/\beta)}{\omega_c}, \tag{6}$$

where ω_c is the gain cross-over frequency of $G(s)$ and PM is the phase margin of $G(s)$. Replacing $G(s)$ given by (4) with

$$\widetilde{G}(s) \doteq \frac{K\,\gamma_1\,\gamma_2\,\gamma_3}{(s+\gamma_1)\,(s+\gamma_2)\,(s+\gamma_3)},$$

similar result is obtained for $\mathscr{S}_{C2}$. □

Proof: $\mathscr{S}_{C1}$ can be decomposed as a feedback system that has a *linear time-invariant* (LTI) element $G(s)$ in the feedforward path and a sector$(0,\beta)$ nonlinearity in the feedback path, where $G(s)$ is given by (4). W.l.o.g., let $|1/\beta| < 1$. By the Circle Theorem [14], this feedback system is stable if and only if $\mathrm{Re}\,G(j\omega) > -1/\beta \quad \forall \omega$.

To derive the upper bound (6) on the tolerable time-delay, observe that the effect of the time-delay is to rotate the Nyquist plot of the feedback loop in the clock-wise direction whilst leaving the magnitude unchanged. So, it suffices to focus on the gain cross-over frequency ω_c, since at that frequency $|G(j\omega_c)| = 1$, and compute the additional phase lag needed to make the system unstable. The phase lag induced by the constant-valued time delay τ at the frequency ω equals $\tau\omega$. Let H denote the hyperplane in the s-plane that is defined as $H \doteq \{x : \mathrm{Re}(x) < -1/\beta\}$. At the gain cross-over frequency, $\measuredangle G(j\omega_c) = -180^\circ + \mathrm{PM}$. Hence, rotating $G(j\omega_c)$ clock-wise through $\theta \doteq \mathrm{PM} - \cos^{-1}(-1/\beta)$ makes it intersect with the hyperplane H, which makes the system $\mathscr{S}_{C1}$ unstable as a consequence of the Circle Theorem. The time-delay that causes this additional phase lag is θ/ω_c. Hence the proof. □

Remark 6. An illustration of the argument used to prove the bound (6) on time-delay is given in Fig. 7. □

Remark 7. Using the logic explained in [11], it readily follows that x_1 and x_2 can be allowed to be real-valued

ISBN: 978-988-14047-9-4
ISSN: 2078-0958 (Print); ISSN: 2078-0966 (Online)

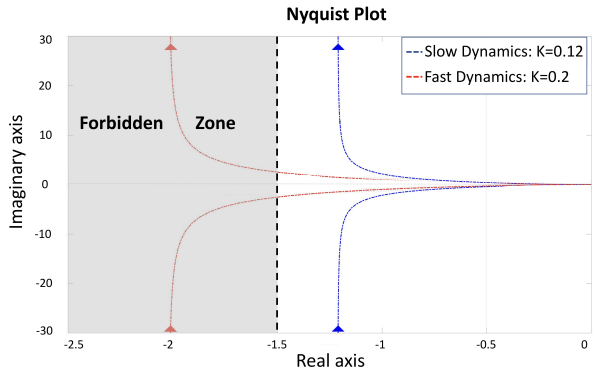

Fig. 6: *An illustration of the finite gain stability analysis of $\mathscr{S}_{C1}$ using our Theorem 1. If the feedback loop is slow enough, the Nyquist plot of the feedback loop is outside the forbidden zone specified by the Circle Criterion and, consequently, $\mathscr{S}_{C1}$ is stable and computes the ratio x_1/x_2 for the given x_1 and x_2. However, if the feedback loop is speeded up to ensure that the circuit computes the ratio faster, the Nyquist plot of the feedback loop enters the forbidden zone and, consequently, $\mathscr{S}_{C1}$ is unstable and cannot compute the ratio x_1/x_2 for the given x_1 and x_2.*

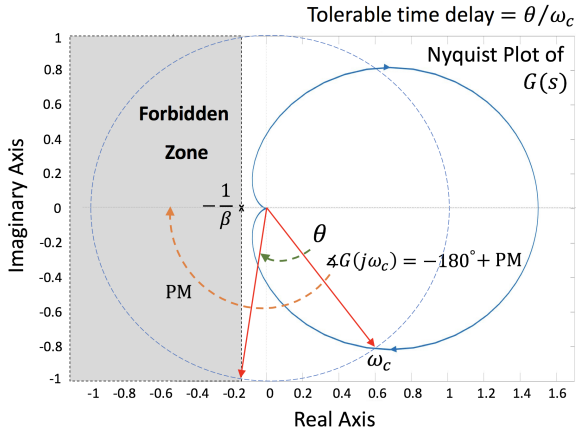

Fig. 7: *A graphical illustration of our derivation of the upper bound (6) on the amount of time delay that can be tolerated by $\mathscr{S}_{C1}$. At the gain cross-over frequency ω_c, $|G(j\omega_c)| = 1$ and $\angle G(j\omega_c) = -180^\circ + PM$. Here, the maximum delay that can be tolerated is $\tau^* = \theta/\omega_c$.*

polynomials as well. □

IV. CONCLUSIONS

We have presented two circuits $\mathscr{S}_{C1}$ and $\mathscr{S}_{C2}$, and their abstract chemical reaction network representations, that accurately compute the ratio of two entities; the entities can be either two constant-valued scalars or two time-varying scalars or two constant-valued polynomials or two time-varying polynomials. We have also characterised their finite gain stability and have derived an upper bound on the time-delay that can be safely tolerated by these circuits.

ACKNOWLEDGMENT

This research is supported, in parts, by the EPSRC INDUSTRIAL CASE AWARD (CASE Voucher 16000070), Microsoft Research, and the EPSRC/BBSRC grant BB/M017982/1 to the Warwick Integrative Synthetic Biology Centre.

REFERENCES

[1] G. Seelig, D. Soloveichik, D. Zhang, and E. Winfree, "Enzyme-free nucleic acid logic circuits," *Science*, vol. 314, no. 5805, pp. 1585–1588, 2006.
[2] D. Zhang, A. Turberfield, B. Yurke, and E. Winfree, "Engineering entropy-driven reactions and networks catalyzed by DNA," *Science*, vol. 318, pp. 1121–1125, 2007.
[3] A. Padirac, T. Fujii, and Y. Rondelez, "Nucleic acids for the rational design of reaction circuits," *Current Opinion of Biotechnology*, vol. 24, pp. 575–580, 2013.
[4] B. Yordanov, J. Kim, R. Petersen, A. Shudy, V. Kulkarni, and A. Philips, "Computational design of nucleic acid feedback control circuits," *ACS Synthetic Biology*, vol. 3, pp. 600–616, 2014.
[5] D. Zhang, "Towards domain-based sequence design for DNA strand displacement reactions," in *DNA Computing and Molecular Programming*, S. Y. and M. Y., Eds. Berlin, Germany: Springer, 2011, vol. 6518, pp. 162–175.
[6] K. Montagne, R. Plasson, Y. Sakai, T. Fujii, and Y. Rondelez, "Programming an *in vitro* DNA oscillator using a molecular networking strategy," *Molecular Systems Biology*, vol. 7, no. 466, pp. 1–7, 2011.
[7] J. Kim and E. Winfree, "Synthetic *in vitro* transcriptional oscillators," *Molecular Systems Biology*, vol. 7, no. 465, 2011.
[8] Y.-J. Chen, N. Dalchau, N. Srinivas, A. Philips, L. Cardelli, D. Soloveichik, and G. Seelig, "Programmable chemical controllers made from DNA," *Nature Nanotechnology*, vol. 8, pp. 755–762, 2013.
[9] T. Fujii and Y. Rondelez, "Predator-prey molecular ecosystems," *ACS Nanotechnology*, vol. 7, no. 1, pp. 27–34, 2013.
[10] D. Soloveichik, G. Seelig, and E. Winfree, "DNA as a universal substrate for chemical kinetics," *PNAS*, vol. 12, pp. 5393–5398, 2010.
[11] M. Foo, J. Kim, R. Sawlekar, D. Bates, G.-B. Stan, and V. Kulkarni, "On the biomolecular implementation of nonlinear system theoretic operators," in *Proceedings of the European Control Conference*, Aalborg, Denmark, June/July 2016.
[12] K. Oishi and E. Klavins, "Biomolecular implementation of linear I/O systems," *IET Systems Biology*, vol. 5, pp. 252–260, 2011.
[13] S. Skogestad and I. Postlethwaite, *Multivariable Feedback Control - Analysis and Design (2nd Edition)*. Chichester, UK: John Wiley & Sons, 2007.
[14] G. Zames, "On the input-output stability of time-varying nonlinear feedback systems: Parts I and II." *IEEE Transactions on Automatic Control*, vol. 11, no. 2/3, pp. 228–238, 465–476, 1966.

V. CORRECTIONS TO THE PRINTED VERSION

On May 9, 2018, the online version of this paper was revised from the printed version as follows: (1) "$\sin^{-1}$(PM)" in the caption of Fig. 7 was corrected to "PM", (2) "$\dot{z}_1 = \delta_2 g$" in Table II was corrected to "$\dot{g} = \delta_2 z_1$", (3) more graphical details were added to Fig. 6 and Fig. 7, (4) the sentence "W.l.o.g., let $|1/\beta| < 1$." was added to the proof of Theorem 1, (5) the sentence "We refer to the blocks B1 and B2 taken together as B1+B2: in other words, the block B1+B2 has x_1 and w as its inputs and produces z_1 as its output." was added to the APPENDIX, and (6) the caption of Fig. 1 was revised slightly to reflect the fifth correction.

APPENDIX

Here, in Table II, we note down the ODE's, ACRNs, and DNA implementation details for $\mathscr{S}_{C1}$. We refer to the blocks B1 and B2 taken together as B1+B2: in other words, the block B1+B2 has x_1 and w as its inputs and produces z_1 as its output. The annihilation reaction rate η is to be chosen arbitrarily large.

TABLE II: Ratio Computation Using $\mathscr{S}_{C1}$: DNA Implementation, the ACRNs and the ODEs

DNA Implementation	Formal CRNs	ODEs
Block B1+B2		
$x_1^\pm + G_1^\pm \xrightarrow{q_1} \emptyset + O_1^\pm$ $O_1^\pm + T_1^\pm \xrightarrow{q_{max}} x_1^\pm + z_1^\pm$	$x_1^\pm \xrightarrow{K\delta_1} x_1^\pm + z_1^\pm$	$\dot{z}_1 = \delta_1(K(x_1 - w) - z_1)$
$w^\mp + G_2^\pm \xrightarrow{q_2} \emptyset + O_2^\pm$ $O_2^\pm + T_2^\pm \xrightarrow{q_{max}} w^\mp + z_1^\pm$	$w^\mp \xrightarrow{K\delta_1} w^\mp + z_1^\pm$	
$z_1^\pm + G_3^\pm \xrightarrow{q_3} \emptyset$	$z_1^\pm \xrightarrow{\delta_1} \emptyset$	
$x_1^+ + L_{1x} \underset{q_{max}}{\overset{q_{max}}{\rightleftharpoons}} H_{1x} + B_{1x}$ $x_1^- + LS_{1x} \underset{q_{max}}{\overset{q_{max}}{\rightleftharpoons}} HS_{1x} + BS_{1x}$ $x_1^- + H_{1x} \xrightarrow{q_{max}} \emptyset$	$x_1^+ + x_1^- \xrightarrow{\eta} \emptyset$	
$w^+ + L_{1w} \underset{q_{max}}{\overset{q_{max}}{\rightleftharpoons}} H_{1w} + B_{1w}$ $w^- + LS_{1w} \underset{q_{max}}{\overset{q_{max}}{\rightleftharpoons}} HS_{1w} + BS_{1w}$ $w^- + H_{1w} \xrightarrow{q_{max}} \emptyset$	$w^+ + w^- \xrightarrow{\eta} \emptyset$	
$z_1^+ + L_{1z} \underset{q_{max}}{\overset{q_{max}}{\rightleftharpoons}} H_{1z} + B_{1z}$ $z_1^- + LS_{1z} \underset{q_{max}}{\overset{q_{max}}{\rightleftharpoons}} HS_{1z} + BS_{1z}$ $z_1^- + H_{1z} \xrightarrow{q_{max}} \emptyset$	$z_1^+ + z_1^- \xrightarrow{\eta} \emptyset$	
Block B3		
$z_1^\pm + G_7^\pm \xrightarrow{q_7} \emptyset + O_7^\pm$ $O_7^\pm + T_7^\pm \xrightarrow{q_{max}} z_1^\pm + g^\pm$	$z_1^\pm \xrightarrow{\delta_2} z_1^\pm + g^\pm$	$\dot{g} = \delta_2 z_1$
$g^+ + L_{3g} \underset{q_{max}}{\overset{q_{max}}{\rightleftharpoons}} H_{3g} + B_{3g}$ $g^- + LS_{3g} \underset{q_{max}}{\overset{q_{max}}{\rightleftharpoons}} HS_{3g} + BS_{3g}$ $g^- + H_{3g} \xrightarrow{q_{max}} \emptyset$	$g^+ + g^- \xrightarrow{\eta} \emptyset$	
Block B4		
$x_2^\pm + L_{3x2}^\pm \underset{q_{max}}{\overset{q_{3'}}{\rightleftharpoons}} H_{3x2}^\pm + B_{3x2}^\pm$ $g^\pm + H_{3g}^\pm \xrightarrow{q_{max}} O_5^\pm$ $O_5^\pm + T_5^\pm \xrightarrow{q_{max}} w^\pm$	$x_2^\pm + g^\pm \xrightarrow{\delta_3} x_2^\pm + g^\pm + w^\pm$	$\dot{w} = \delta_3(x_2 * g - w)$
$w^\pm + G_6^\pm \xrightarrow{q_6} \emptyset$	$w^\pm \xrightarrow{\delta_3} \emptyset$	
$x_2^+ + L_{1x2} \underset{q_{max}}{\overset{q_{max}}{\rightleftharpoons}} H_{1x2} + B_{1x2}$ $x_2^- + LS_{1x2} \underset{q_{max}}{\overset{q_{max}}{\rightleftharpoons}} HS_{1x2} + BS_{1x2}$ $x_2^- + H_{1x2} \xrightarrow{q_{max}} \emptyset$	$x_2^+ + x_2^- \xrightarrow{\eta} \emptyset$	

ISBN: 978-988-14047-9-4
ISSN: 2078-0958 (Print); ISSN: 2078-0966 (Online)